Journal of Materials Chemistry A

PAPER

View Article Online
View Journal | View Issue

Cite this: J. Mater. Chem. A, 2015, 3, 14157

An In^{III}-based anionic metal–organic framework: sensitization of lanthanide (III) ions and selective absorption and separation of cationic dyes†

Lin Liu,[a] Xiao-Nan Zhang,[a] Zheng-Bo Han,*[a] Ming-Liang Gao,[a] Xiao-Man Cao[a] and Shi-Ming Wang*[b]

Received 6th February 2015
Accepted 27th May 2015

DOI: 10.1039/c5ta00986c

www.rsc.org/MaterialsA

An In^{III}-based anionic framework (In^{III}-MOF) with 4-connected $SrAl_2$ topology was constructed. The In^{III}-MOF with permanent porosity functions as a host for encapsulation of Ln^{3+} ions through ion-exchange processes. The photophysical properties of the as-prepared Ln^{3+}@In^{III}-MOF were investigated and the results showed that the In^{III}-MOF could serve as an antenna to sensitize Ln^{3+} cations, especially suitable for Tb^{3+} and Eu^{3+} ions. The possible sensitization mechanism has been studied by surface photovoltage spectroscopy. Additionally, the In^{III}-MOF could also act as a host material when applied in the separation and purification of cationic dyes, which is highly based on the size and charge of organic dyes. Moreover, it can be used as a chromatographic column stationary phase to separate cationic dyes more efficiently and selectively. It is believed that the as-prepared In^{III}-MOF may have potential applications in optical materials and environmental fields.

Introduction

Metal–Organic Frameworks (MOFs) have been widely investigated as functional materials in supramolecular chemistry, such as gas storage, ion-exchange, separation and fluorescent sensors.[1] In particular, MOFs could provide a potential platform whose functions can be tuned through rational postsynthetic modification.[2] Particularly, charged MOFs make the post-synthetic modification facile and controllable.[3]

Lanthanide-based luminescent materials usually generate sharp fluorescent emissions with different colors. Therefore, engineering lanthanide-based MOFs is a sensible choice to obtain tunable luminescent materials.[4] One way is using lanthanide ions as metal nodes for MOFs[5] and light emission with different colors could be achieved by altering the lanthanide ions of the isomorphic frameworks.[6] Another way is encapsulating the lanthanide ions into stable MOFs through a postsynthetic process, which provides access to the tunable luminescent materials by means of controlling different types of guest species.[7] Very recently, anionic MOFs have been reported to provide an efficient medium to capture and sensitize lanthanide cations to achieve luminescent materials with different colors.[8] Notably, primary color light emissions were obtained by this simple method. When mixed, the two (blue and yellow) or three (blue, green, and red) primary colors together would generate white light emission.[9] It is judicious to choose lanthanide cations as the guest for anionic frameworks to obtain primary color emission. Petoud and co-workers reported porous anionic bio-MOF-1 which can incorporate lanthanide cations *via* a cation-exchange process and sensitize multiple lanthanide cations, thus allowing for the facile preparation of multiple different luminescent materials.[8a] Such progress in this field permits us to rationally design and synthesize ionic MOFs for use as specific host–guest materials.

In addition, charged MOFs can be applied in absorption and separation of metal cations, as well as show great potential in the efficient separation of organic dyes.[3c,10] In particular, charged MOF based ion-exchange chromatograph and ion-exchange solid phase extraction would be powerful tools for charged molecule separation.[11] However, only a few examples of the application of charged MOFs as ion-exchange chromatographs for dyes have been reported.[12] Bu and co-workers reported positive frameworks, which could aid in the selective separation of anionic dye molecules.[12a] The selective separation of dyes is based on the following reasons: first, the counter ions could only be substituted by the same charged dye molecules; second, the pore size would determine what size of dyes could be used as the guests for the framework. Therefore, the reasonable selection of the ligand and metal node would be the crucial factor to construct a charged framework with multi-functions.

[a]College of Chemistry, Liaoning University, Shenyang 110036, P. R. China. E-mail: ceshzb@lnu.edu.cn

[b]College of Light Industry, Liaoning University, Shenyang 110036, P. R. China. E-mail: wangsm383@163.com

† Electronic supplementary information (ESI) available: The luminescence spectrum of the H_4L ligands, the TG curves of the In^{III}-MOF, the PXRD patterns of the In^{III}-MOF, and more information about the crystal structures. CCDC 1045476. For ESI and crystallographic data in CIF or other electronic format see DOI: 10.1039/c5ta00986c

Until now, there are a number of reports on In^{III}-based ionic frameworks. Most of the In^{III}-based frameworks are highly stable and show advanced functions.[10d,13] Exploring new In^{III}-based anionic frameworks is desirable. In this paper, an anionic framework with the formula of $[(CH_3)_2NH_2][In(L)]\cdot CH_3CH_2OH$ (In^{III}-MOF) (H_4L = 2,3′,5,5′-biphenyl tetracarboxylic acid) was prepared by utilizing a solvothermal method. The In^{III}-MOF could undergo an ion-exchange process to encapsulate the lanthanide cations and separate cationic dyes. The In^{III}-MOF could serve as an antenna to sensitize Ln^{3+} cations, especially suitable for Tb^{3+} and Eu^{3+} ions. The mechanism of MOF sensitization of Ln^{3+} luminescence was first investigated by surface photovoltage spectroscopy technology in this work. Additionally, the In^{III}-MOF presents excellent revisable absorption of cationic dyes and can serve as a chromatographic column stationary phase to separate cationic dye molecules efficiently and selectively.

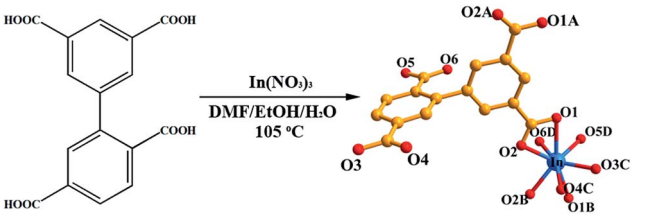

Scheme 1 Schematic representation of the synthesis of the In^{III}-MOF. Symmetry codes: (A) x, 1.5 − y, z; (B) 0.5 − x, 1 − y, 0.5 + z; (C) 0.5 − x, 1 − y, 0.5 + z; (D) 1 − x, 1 − y, 1 − z.

Experimental section

Materials and methods

All starting materials and solvents employed were commercially available and used without further purification. X-ray powder diffraction was recorded with a Bruker AXS D8 advanced automated diffractometer with Cu-Kα radiation. Thermogravimetric analyses (TGA) were carried out on a Perkin-Elmer Pyrisl (25–700 °C, 5 °C min^{-1}, flowing N_2 (g)). Ar adsorption–desorption experiments were carried out on an automated gas sorption analyzer (Quantachrome Instrument ASiQ-C). The C, H, and N microanalyses were carried out with a Perkin-Elmer 240 elemental analyzer. Inductively coupled plasma-optical emission spectroscopy (ICP) was performed using a 700 Series ICP-OES (Agilent Technologies). The FT-IR spectra were recorded from KBr pellets in the range of 4000–400 cm^{-1} on a Nicolet 5DX spectrometer. Luminescence spectra and lifetimes of the solid samples were investigated with an FLSP920 Edinburgh Fluorescence Spectrometer at room temperature. The surface photovoltage spectroscopy measurement was performed on a lab-made instrument, which constitutes a source of monochromatic light, a lock-in amplifier (SR830-DSP) with a light chopper (SR540) and a photovoltaic cell. A 500 W xenon lamp (CHFXQ500 W, Global xenon lamp power) and a double-prism monochromator (Hilger and Watts, D300) provided monochromatic light. The construction of the photovoltaic cell was a sandwich-like structure of ITO-sample-ITO. All UV-vis spectra were measured on a SP-752(PC) UV-vis spectrophotometer (Shanghai Spectrum Instrument Co., Ltd).

Preparation of $[(CH_3)_2NH_2][In(L)]\cdot CH_3CH_2OH$ (In^{III}-MOF)

A mixture of $In(NO_3)_3$ (15 mg, 0.16 mmol), H_4L (5 mg, 0.15 mmol), DMF/CH_3CH_2OH/H_2O (2 : 1 : 1, 2 mL) and one drop of 16 M HNO_3 was stirred in a glass vial for *ca.* 20 min at room temperature, which was then heated in an oven to 378 K for 3 days, followed by slow cooling (5 K h^{-1}) to room temperature (Scheme 1). A colorless stick-like crystal In^{III}-MOF was obtained and washed with DMF and dried in air (yield: *ca.* 53%). The counter cation $(CH_3)_2NH_2^+$ is generated *via* decomposition of the DMF solvent. Elemental analysis calcd (%) for the In^{III}-MOF, $C_{20}H_{20}InNO_9$ (%): C 45.05, H 3.78, and N 2.63; found: C 45.56, H 3.56, and N 2.43; IR (KBr pellets, cm^{-1}): 3451 (s), 2915 (w) 1665 (vs), 1587 (s), 1385 (vs), 1266 (m), 1096 (m), 862 (m), 759 (m), 664 (w), 554 (m). The composition of the In^{III}-MOF was confirmed by single crystal X-ray diffraction, elemental analysis and IR spectroscopy; in addition, the phase purity of the bulk sample was confirmed by powder X-ray diffraction (PXRD).

X-ray crystallography

Crystallographic data of the complex were collected at 293 K with a Apex CCD II diffractometer with Mo-Kα radiation (λ = 0.71073 Å) and a graphite monochromator using the ω-scan mode. The structure was solved by direct method and refined on F^2 by full-matrix least squares using the SHELXTL-97 crystallographic software package.[14] $(CH_3)_2NH_2^+$ cations and guest solution molecules were highly disordered, and attempts to locate and refine the peaks were unsuccessful. The diffused electron densities resulting from these residual molecules were removed from the dataset using the SQUEEZE[15] routine of PLATON and refined further using the data generated. The contents of $(CH_3)_2NH_2^+$ and guest molecules are not represented in the unit cell contents of the crystal data. Crystallographic data for structural analyses are summarized in Table S1.†

Encapsulation of Ln^{3+} cations in In^{III}-MOF

$Ln(NO_3)_3$[$Sm(NO_3)_3\cdot 6H_2O$, $Eu(NO_3)_3\cdot 6H_2O$, $Tb(NO_3)_3\cdot 5H_2O$, and $Dy(NO_3)_3\cdot 5H_2O$] was used as purchased. A solution of $Ln(NO_3)_3$ in DMF (0.1 M) was prepared. Encapsulation of Ln^{3+} cations was performed as follows: the as-synthesized In^{III}-MOF was soaked in the $Ln(NO_3)_3$ solution and changed every 24 h with fresh solution for 3 days. After cation exchange was completed, the materials were thoroughly washed with DMF and soaked in DMF for at least 24 h.

Experimental details for organic dye selective adsorption and separation

The freshly prepared In^{III}-MOF (20 mg) was immersed in 5 mL DMF solutions of different organic dyes with concentrations of 5×10^{-5} M. The release experiment was carried out after the completion of an ion-exchange process of Methylene blue (MB)

on the In^{III}-MOF. Then, the as-prepared MB^+@In^{III}-MOF was immersed in the saturated solution of NaCl in DMF with the same volume. The chromatographic column is made of a bottomless NMR sample tube (Ø5 mm, 180 mm) and the In^{III}-MOF was filled in the NMR sample tube (80 mm) as the stationary phase. The DMF solutions of MB^+, and mixed MB^+/MO^- (1 : 1), MB^+/SD^0 (1 : 1), and MB^+/CV^+ (1 : 1) (10^{-4} M, 3 mL) were used for separation.

Results and discussion

Crystal structure of In^{III}-MOF

The single-crystal X-ray analysis reveals that the In^{III}-MOF features a three-dimensional framework constructed from mononuclear $[In(O_2CR)_4]$ nodes bridged by the tetracarboxylate ligand (L) (Fig. 1a). The counterions of $(CH_3)_2NH_2^+$ are located in the channels to balance the charge. In the anionic framework, the four carboxylate groups of the L ligand adopt chelating coordination mode to link four In^{III} ions. The In^{III} ion is eight-coordinate and surrounded by eight oxygen atoms from four individual L ligands. There are two different kinds of channels along the *b*-axis: the smaller quadrilateral channels of 5.22 × 6.85 Å^2 and larger quadrilateral channels of 9.17 × 14.43 Å^2 (measured between opposite atoms) in size (Fig. S1†). The total accessible volume of the In^{III}-MOF after the removal of the counter cations and guest solvent molecules is *ca.* 65.5% using PLATON.[16] However, this void contains the disordered $(CH_3)_2NH_2^+$ cations and guest solvent molecules. The $(CH_3)_2NH_2^+$ cations are difficult to remove after thermal activation, which give rise to the Ar uptake that is relatively small (Fig. S2†). Therefore, a Li^+-exchanged sample In^{III}-MOF-Li^+ was prepared by immersing crystals of the In^{III}-MOF in a saturated solution of LiCl in DMF. As shown in Fig. S6,† both Ar isotherms of the In^{III}-MOF and In^{III}-MOF-Li^+ exhibit typical Type-I adsorption behaviour, confirming the retention of the microporous structures of the crystalline samples. The BET surface areas of the In^{III}-MOF and In^{III}-MOF-Li^+ were estimated to be 182.8 and 554.1 m^2 g^{-1}, respectively, indicating that the adsorption capacity of the In^{III}-MOF-Li^+ increases significantly. From the topological point of view, if the L ligands and In^{III} ions are considered as 4-connected nodes, the 3D structure of the In^{III}-MOF can be simplified as a uninodal four-connected SRA topology with a Schläfli symbol of $4^2 \cdot 6^3 \cdot 8$, which is related to the structural prototype of $SrAl_2$ (or zeolite ABW)[17] (Fig. 1b).

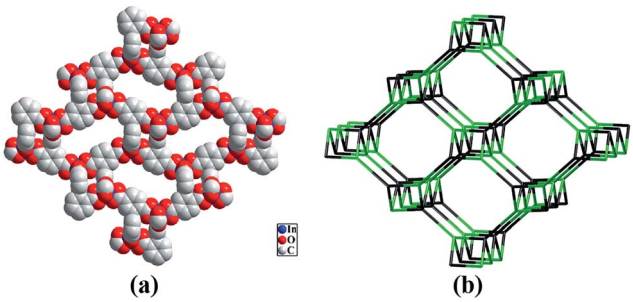

Fig. 1 (a) Space-filling representation of the In^{III}-MOF along the *b*-axis; (b) view of the 3D four-connected framework of the In^{III}-MOF which can be represented as a four-connected net of SRA topology (the green nodes represent the In nodes and the black nodes represent the L_4 ligands).

Thermal stability

The TGA curve of the In^{III}-MOF displayed that the weight loss of the guest solvent molecules was well resolved (Fig. S3†). The curve exhibits two major losses in the temperature range of 25–500 °C, the weight loss of 17.3% during the first step between 25 and 250 °C corresponds to the loss of one guest CH_3CH_2OH molecule and one free $(CH_3)_2NH_2^+$ cation (calculated 17.3%). Decomposition of the In^{III}-MOF began above 330 °C. The powder X-ray diffraction (PXRD) pattern of the In^{III}-MOF shows that the diffraction peaks of both simulated and experimental patterns match well in key positions, indicating the phase purity of the In^{III}-MOF (Fig. S4†). Additionally, the In^{III}-MOF shows favorable water stability (Fig. S5†), which is crucial for the development of its porous system in relevant applications.

Luminescent properties

Because of the anionic framework of the In^{III}-MOF and $(CH_3)_2NH_2^+$ in the 1D channels, the In^{III}-MOF is suitable for the exchange of lanthanide cations to the host framework to form novel Ln-doped luminescent materials and new Ln^{3+} sensors through the antenna effect.[4a] We tried to introduce lanthanide cations into the pores of the In^{III}-MOF and then analyze the luminescent properties of the resulting Ln^{3+}@In^{III}-MOF. ICP data of the Ln^{3+} exchanged materials revealed the doped amounts of the Ln^{3+} ions (Table S2†). The molar ratio of In^{3+}/Ln^{3+} was about 3 : 1, which suggested that one Ln^{3+} ion exchanged out approximately three $(CH_3)_2NH_2^+$ cations. The PXRD patterns (Fig. S6†) and IR spectra (Fig. S7†) of the Ln^{3+}@In^{III}-MOF confirmed that the structure of the In^{III}-MOF maintained its crystalline integrity after the ion-exchange experiments. As expected, the In^{III}-MOF succeeds in sensitizing Tb^{3+}, Sm^{3+}, Eu^{3+}, and Dy^{3+}, which is confirmed from the emission spectra of the Ln^{3+}@In^{III}-MOF. The excitation and emission spectra of the powder samples of H_4L are displayed in Fig. S8.† The emission spectrum of the In^{III}-MOF is shown in Fig. 2a. The H_4L ligand exhibits strong emission at 420 nm with the excitation at 363 nm due to π–π* transitions. The In^{III}-MOF exhibits more enhanced blue light emission and shifts slightly to 447 nm with the excitation at 340 nm. Under the excitation at 340 nm, the Ln^{3+}@In^{III}-MOF (Ln^{3+} = Tb^{3+}, Eu^{3+}, Sm^{3+} and Dy^{3+}) samples show a similar emission in the region of 400–500 nm with different intensities. The emission spectrum of the Tb^{3+}@In^{III}-MOF emits its distinctive green color with typical Tb^{3+} ion emissions at λ_{em} = 489, 544, 583 and 622 nm (Fig. 2b), which correspond to the characteristic $^5D_4 \rightarrow {}^7F_J$ (J = 3–6) transitions. Two intense emission bands at λ_{em} = 489 and 544 are due to the $^5D_4 \rightarrow {}^7F_6$ and $^5D_4 \rightarrow {}^7F_5$ transitions and the weaker emission bands at λ_{em} = 583 and 622 nm originate from the $^5D_4 \rightarrow {}^7F_4$ and $^5D_4 \rightarrow {}^7F_3$ transitions. This phenomenon is

associated with the decrease of the emission intensity of the In^{III}-MOF at ~447 nm, and it is less pronounced as compared with the Tb^{3+} ion emissions. This result confirmed the efficient energy transfer from the In^{III}-MOF to the Tb^{3+} centers. The spectrum is dominated by the $^5D_4 \rightarrow {}^7F_5$ intense band and this is responsible for the brilliant green emission of the Tb^{3+}@In^{III}-MOF hybrid. On the other hand, the emission spectrum of the Eu^{3+}@In^{III}-MOF emits its unique red color with characteristic emissions of the Eu^{3+} ion. As shown in Fig. 2c, the emission spectrum at $\lambda_{em} = 591$, 613, 650, and 699 nm is according to the typical Eu^{3+} ion emission which can originate from the characteristic emission $^5D_0 \rightarrow {}^7F_J$ ($J = 1$–4) transitions. At the same time, the characteristic emission of the In^{III}-MOF at $\lambda_{em} = 447$ still existed. The intense emission bands at $\lambda_{em} = 613$ nm are due to the $^5D_0 \rightarrow {}^7F_2$ transition. These results suggest that only part of the energy is transferred from the In^{III}-MOF to the Eu^{3+} centers. Whereas, the Sm^{3+}@In^{III}-MOF shows two weak characteristic emissions at $\lambda_{em} = 596$ and 644 nm (Fig. 2d), which are typical Sm^{3+} ion emissions and correspond to the characteristic $^4G_{5/2} \rightarrow {}^6H_J$ ($J = 7/2$, 9/2) transitions. Similar to this situation, the emission spectrum of the Dy^{3+}@In^{III}-MOF emits a weak typical Dy^{3+} ion emission at $\lambda_{em} = 572$ nm (Fig. 2e), which can be attributed to the characteristic emission $^4F_{9/2} \rightarrow {}^6H_{13/2}$. These results indicate that the In^{III}-MOF not only acts as a host to encapsulate Ln^{3+} cations, but also serves as an antenna to sensitize Ln^{3+} cations, especially suitable for Tb^{3+} and Eu^{3+}. Thus, the emission color is modulated by the postsynthetic process of encapsulating different Ln^{3+} ions, which may gain white light emission. The corresponding CIE chromaticity coordinates diagram is shown in Fig. 2f. It is noteworthy that the Tb^{3+}@In^{III}-MOF and the Eu^{3+}@In^{III}-MOF show very long Ln^{3+} lifetimes. For example, $\tau = 919.63$ μs for the Tb^{3+}@In^{III}-MOF; $\tau = 362.55$ μs for the Eu^{3+}@In^{III}-MOF. However, the lifetimes of the In^{III}-MOF, Sm^{3+}@In^{III}-MOF and Dy^{3+}@In^{III}-MOF are relatively short ($\tau = 6.83733$ ns for the In^{III}-MOF; $\tau = 1.30488$ ns for the Sm^{3+}@In^{III}-MOF; $\tau_1 = 1.17343$ ns and $\tau_2 = 7.46201$ ns for the Dy^{3+}@In^{III}-MOF). When illuminated with a standard laboratory UV lamp ($\lambda_{ex} = 254$ nm), the doped materials displayed strong luminescence which can be easily observed by the naked eye.

The surface photovoltage spectroscopy (SPS) technique was used for investigating the photophysics of the excited states and the surface charge behavior of the materials. It is an efficient method to reveal the fundamental feature of separation and transport of photogenerated charges.[18] The possible sensitization mechanism for the above phenomenon is proposed as follows. The SPS spectra of the as-prepared In^{III}-MOF and Ln^{3+}@In^{III}-MOF samples are shown in Fig. 3. The In^{III}-MOF presents a positive SPV response band in the region of 300–400 nm and the photovoltage response centered at 329 nm. This indicates that the In^{III}-MOF possesses semiconductor characteristics. When the light illuminated the surface of the In^{III}-MOF, the electrons (e^-) in the valence band (VB) were excited to the conduction band (CB), and holes (h^+) were left in the VB. Driven by the built-in field, the electrons and holes move in opposite directions, which results in different expressions of the surface potential, generating a photovoltage signal. With

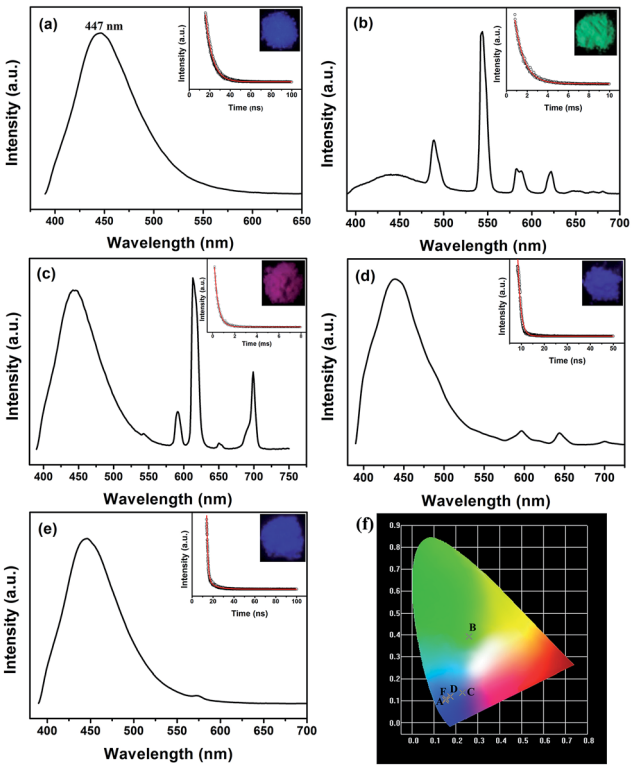

Fig. 2 Emission spectra of (a) In^{III}-MOF, (b) Tb^{3+}@In^{III}-MOF, (c) Eu^{3+}@In^{III}-MOF, (d) Sm^{3+}@In^{III}-MOF and (e) Dy^{3+}@In^{III}-MOF excited at 340 nm in the solid state at room temperature. Insets: luminescence decay curves of (a) In^{III}-MOF, (b) Tb^{3+}@In^{III}-MOF, (c) Eu^{3+}@In^{III}-MOF, (d) Sm^{3+}@In^{III}-MOF and (e) Dy^{3+}@In^{III}-MOF; photographs of the respective samples under a UV lamp; (f) CIE chromaticity diagram of In^{III}-MOF (A) and Ln^{3+}@In^{III}-MOF (Tb^{3+} for B, Eu^{3+} for C, Sm^{3+} for D, and Dy^{3+} for E).

the encapsulation of Ln^{3+} ions, the intensities of the SPS response decrease obviously. The weakened SPS response demonstrates that only a small part of the photogenerated charges are separated, while most of the other photogenerated charges are involved in the sensitization process in Ln^{3+}@In^{III}-MOF samples, which due to the intensity of SPS reflects the separation efficiency of photogenerated charges.[19] As shown in Scheme 2, for the Tb^{3+}@In^{III}-MOF, the energy level of the conduction band of the In^{III}-MOF is higher than that of the emitting state ($^5D_4$) of Tb^{3+} ions. Thus, the photogenerated electrons can transfer to the 5d level of Tb^{3+}. At the same time, holes are inclined to transfer to the 4f level, resulting in improved photoluminescence performance through a radiative transition process. That is to say, Tb^{3+} ions act as recombination centers to accelerate the process of recombination, which facilitates the electron transfer from the In^{III}-MOF to Ln^{3+}. However, a different Ln^{3+}@In^{III}-MOF results in a different SPS response and the intensity of the SPS is consistent with the degree of Ln^{3+} ions sensitized by the In^{III}-MOF. This might be attributed to the different match degrees of the energy level between Ln^{3+} ions and the In^{III}-MOF. In this context, the SPS results provide convincing evidence for the sensitization of Ln^{3+} by the In^{III}-MOF.

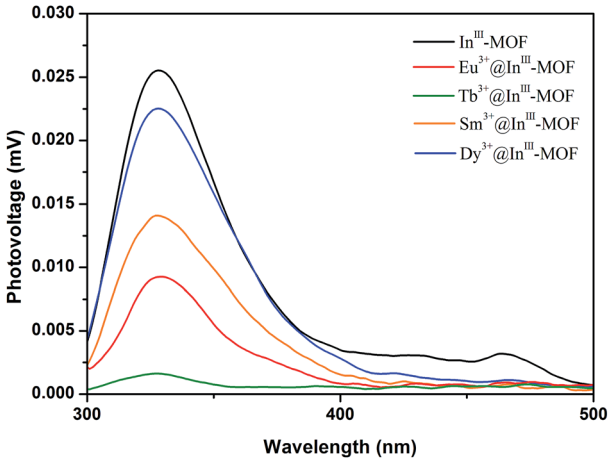

Fig. 3 SPS of In^{III}-MOF and Ln^{3+}@In^{III}-MOF samples.

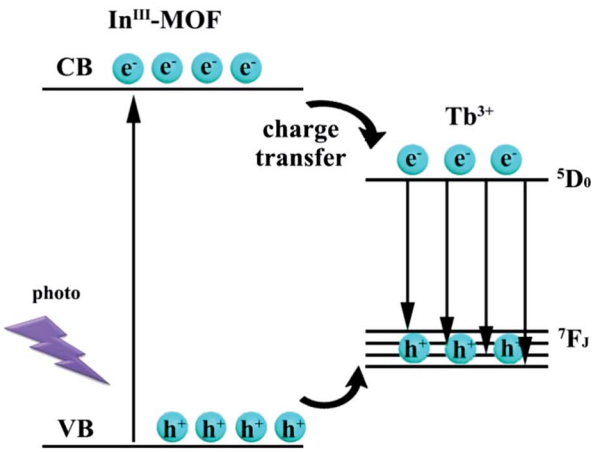

Scheme 2 Transfer and separation of photogenerated charges in Tb^{3+}@In^{III}-MOF.

Organic dye selective adsorption and separation

Currently, dyes are widely used in many industries and the removal of dyes from waste water has been attracting intense attention from an environmental point of view.[20] To investigate the capacity of the In^{III}-MOF in the separation of dye molecules, we used the In^{III}-MOF to capture dyes in DMF solutions. During the dye adsorption and separation process, the charge and size of the organic dye are the two most important factors.[12a] We have chosen four organic dyes for this study: Methylene blue (MB$^+$), Sudan I (SD^0), Methyl orange (MO$^-$) and Crystal Violet (CV$^+$) (Scheme 3). First, we selected MB$^+$, SD^0 and MO$^-$ to investigate the absorption of organic dyes. These dyes feature similar size and molecular weight but different charges (Table 1). The fresh as-prepared In^{III}-MOF was immersed in the DMF solution of MB$^+$, SD^0 and MO$^-$ without disturbance. The content of dye in the solution was detected at certain time intervals using UV-vis absorption spectroscopy. As shown in Fig. 4a and 5, the Abs peak value of the solution declined gradually up to 22 h, suggesting that nearly all the MB$^+$ was absorbed by the In^{III}-MOF. At the same time, the color of the solution fades to transparent. In contrast, no change in the colors of MO$^-$ (Fig. S9†) and SD^0 (Fig. S10†) solutions was detected . What is more, in order to further demonstrate the selective adsorption of MB$^+$ by the In^{III}-MOF, the mixtures of MB$^+$/SD^0 and MB$^+$/MO$^-$ solutions were used. As shown in Fig. 4b and c, the results were as expected: only the MB$^+$ was absorbed by the In^{III}-MOF in the solution mixture and the solutions exhibited the colors of SD^0 and MO$^-$ at last and the color of the In^{III}-MOF changed from colorless to blue. This phenomenon was attributed to the free $(CH_3)_2NH_2^+$ cations present in the channel of the In^{III}-MOF. Therefore, the In^{III}-MOF was only capable of adsorbing cationic dyes through ion-exchange and could not adsorb neutral and anionic dyes. Organic dyes with similar sizes but different charges could be selectively separated utilizing ion-exchange processes.

In order to study the size effect, two kinds of cationic dyes with different sizes were chosen: MB$^+$ and CV$^+$. They have the same charges but different molecular sizes. CV$^+$ takes on a larger appearance (Table 1). Typically, the fresh crystalline samples of the In^{III}-MOF were immersed into DMF solutions of MB$^+$ and CV$^+$ and the concentration changes were monitored by UV-vis absorbance at different time intervals. As shown in Fig. 4a and S11,† for the smaller size MB$^+$, the concentration of the solution declined sharply. However, for the large size CV$^+$, a totally different situation is observed as there is almost no change in the concentration of CV$^+$ in DMF. The size selective

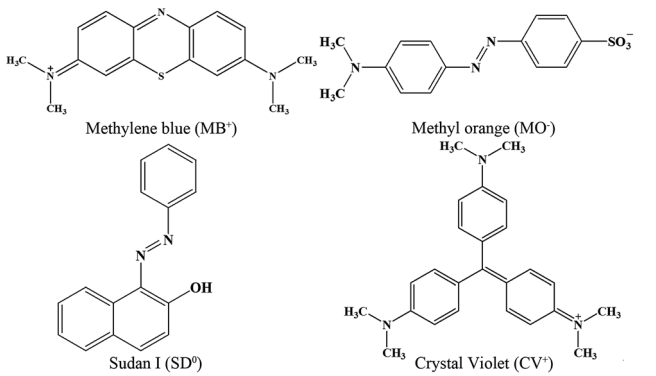

Scheme 3 Chemical structures of MB$^+$, MO$^-$, SD^0 and CV$^+$.

Table 1 Molecular weight and dimensions of different dye molecules

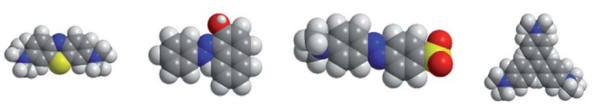

Abbr.	MB$^+$	SD^0	MO$^-$	CV$^+$
M_w	284.40	248.28	304.33	372.53
x (Å)	4.00	3.68	5.31	4.00
y (Å)	7.93	9.74	7.25	16.32
z (Å)	16.34	13.55	17.39	14.15

effect was also tested under mixed solution of MB^+/CV^+. As shown in Fig. 4d, only characteristic peaks of MB^+ decreased significantly. Accordingly, only MB^+ was exchanged by the In^{III}-MOF and the crystal color also changed from colorless to blue, meanwhile the solution changed from blue-violet to purple. The molecular dimensions of the MB^+ dye are 4.00 and 7.93 Å along the x and y directions, respectively, which are much smaller than the diameter of the channel of the In^{III}-MOF (9.17 × 14.43 Å). Thus, MB^+ can enter into the channel of the In^{III}-MOF smoothly. With respect to the CV^+, the molecular dimensions along the x and y directions are 4.00 and 16.32, respectively, which are much larger than the diameter of the channel of the In^{III}-MOF. As a result, CV^+ can not finish the ion-exchange process with the In^{III}-MOF. Such an observation again indicated that the ion-exchange process is size-dependent, which is controlled by the size of the organic dye. If the dye is too large to diffuse into the channel of the In^{III}-MOF, ion-exchange cannot be completed.

The reversibility and stability of the In^{III}-MOF after dye absorption and desorption are also important criteria for real use. The dye release experiments were also carried out using the MB^+@In^{III}-MOF. Typically, the MB^+@In^{III}-MOF was soaked in the saturated NaCl DMF solution and we used the UV-vis spectrum for detecting the concentration of dye in the solution. As shown in Fig. 5 and S12,† the concentration of MB^+ in DMF solution increased gradually. The solution changed from colorless to blue color and the color of the crystal turned back to colorless. This phenomenon is attributed to the ion exchange process, which is reversible and based on the dynamic equilibrium between different guests.[12a] As a result, the Na^+ could enter into the channel of the In^{III}-MOF instead of MB^+ when the concentration of the Na^+ cation is large enough. The PXRD of the In^{III}-MOF after the release experiment confirmed the stability of the host crystal material (Fig. S13†). It can be concluded that the skeleton of the In^{III}-MOF did not change after the dye release. High efficiency selective absorption of dyes inspired us to use the In^{III}-MOF as the stationary phase of an ion chromatographic column. The solution of MB^+ and mixed solutions of MB^+/MO^-, MB^+/SD^0 and MB^+/CV^+ with the same concentration were injected into the chromatographic column, respectively. After the injection, we took photos of the columns 3 minutes later. As shown in Fig. 6, MB^+ is quickly adsorbed onto the In^{III}-MOF and remained at the top of the chromatographic column (Fig. 6b), while MO^- (Fig. 6c), SD^0 (Fig. 6d) and CV^+ (Fig. 6e) were transported through the column, thus resulting in the separation. This phenomenon could be easily observed by the naked eye. From the above experiments, we can further deduce that the In^{III}-MOF could serve as a good adsorbent to remove cationic dye molecules efficiently and selectively.

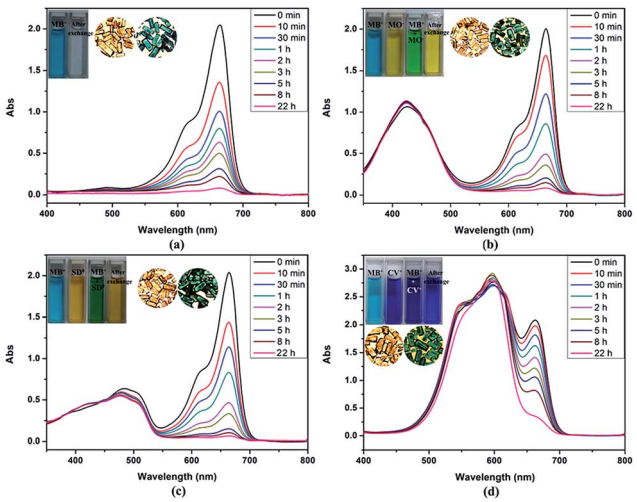

Fig. 4 UV-vis spectra of DMF solutions of equimolar dyes in the presence of the In^{III}-MOF monitored with time: (a) MB^+, (b) MB^+/MO^-, (c) MB^+/SD^0, and (d) MB^+/CV^+. The photographs show the colors of the dye solutions and the crystalline samples of the In^{III}-MOF, before and after ion-exchange for 22 h.

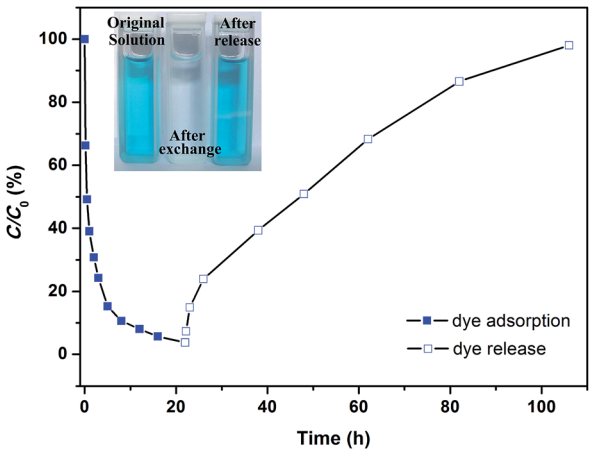

Fig. 5 The reversible absorption and release of MB^+ in a full ion-exchange and release cycle.

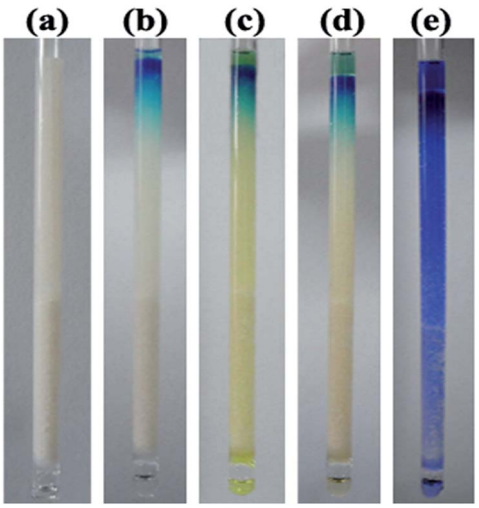

Fig. 6 Photograph of the as-prepared In^{III}-MOF-filled chromatographic column (a); separation process for MB^+ (b), MB^+/MO^- (c), MB^+/SD^0 (d), and MB^+/CV^+ (e).

Conclusion

In summary, a new anionic In^{III}-based porous MOF with $SrAl_2$ topology has been synthesized and characterized, which is an excellent host for encapsulation and sensitization of Ln^{3+} cations, especially suitable for Tb^{3+} and Eu^{3+} ions, and presents highly selective absorption and separation of cationic dyes *via* ion-exchange processes. The mechanism of In^{III}-MOF sensitization of Ln^{3+} luminescence was investigated by the SPS technology, which indicated that the Ln^{3+} ions act as electronic recombination centers and accelerate electron transfer from the In^{III}-MOF to Ln^{3+}. In addition, the In^{III}-MOF can be used as an ion chromatographic stationary phase for the selective separation of cationic organic dyes, which could be applied in environmental fields. Ongoing work is focused on applying ionic frameworks *via* the ion-exchange process to fabricate functional materials with versatile properties for use in catalysis, adsorption, separation, luminescent materials, devices, *etc.*

Acknowledgements

This work was granted financial support from the National Natural Science Foundation of China (Grant 20871063, 21271096) and the Liaoning Natural Science Foundation, China (20141052).

Notes and references

1 (*a*) H. Furukawa, N. Ko, Y. B. Go, N. Aratani, S. B. Choi, E. Choi, A. O. Yazaydin, R. Q. Snurr, M. O'Keeffe, J. Kim and O. M. Yaghi, *Science*, 2010, **329**, 424–428; (*b*) M. Eddaoudi, D. F. Sava, J. F. Eubank, K. Adil and V. Guillerm, *Chem. Soc. Rev.*, 2015, **44**, 228–249; (*c*) D. Maspoch, D. Ruiz-Molina, K. Wurst, N. Domingo, M. Cavallini, F. Biscarini, J. Tejada, C. Rovira and J. Veciana, *Nat. Mater.*, 2003, **2**, 190–195; (*d*) S. Stepanow, M. Lingenfelder, A. Dmitriev, H. Spillmann, E. Delvigne, N. Lin, X. Deng, C. Cai, J. V. Barth and K. Kern, *Nat. Mater.*, 2004, **3**, 229–233; (*e*) S. Horike, S. Shimomura and S. Kitagawa, *Nat. Chem.*, 2009, **1**, 695–704.

2 (*a*) M. Banerjee, S. Das, M. Yoon, H. J. Choi, M. H. Hyun, S. M. Park, G. Seo and K. Kim, *J. Am. Chem. Soc.*, 2009, **131**, 7524–7525; (*b*) T. Gadzikwa, O. K. Farha, K. L. Mulfort, J. T. Hupp and S. T. Nguyen, *Chem. Commun.*, 2009, 3720–3722; (*c*) B. Li, Y. Zhang, D. Ma, L. Li, G. Li, G. Li, Z. Shi and S. Feng, *Chem. Commun.*, 2012, **48**, 6151–6153; (*d*) V. Valtchev, G. Majano, S. Mintova and J. Perez-Ramirez, *Chem. Soc. Rev.*, 2013, **42**, 263–290; (*e*) M. H. Zeng, Z. Yin, Y. X. Tan, W. X. Zhang and Y. P. He, *J. Am. Chem. Soc.*, 2014, **136**, 4680–4688.

3 (*a*) N. Ko, K. Noh, S. Sung, H. J. Park, S. Y. Park and J. Kim, *Chem. Commun.*, 2014, **50**, 6785–6788; (*b*) C. Mao, R. A. Kudla, F. Zuo, X. Zhao, L. J. Mueller, X. Bu and P. Feng, *J. Am. Chem. Soc.*, 2014, **136**, 7579–7582; (*c*) Y. X. Tan, Y. P. He and J. Zhang, *Chem. Commun.*, 2014, **50**, 6153–6156; (*d*) J. Yu, Y. Cui, C. Wu, Y. Yang, Z. Wang, M. O'Keeffe, B. Chen and G. Qian, *Angew. Chem., Int. Ed.*, 2012, **51**, 10542–10545; (*e*) J. Yu, Y. Cui, H. Xu, Y. Yang, Z. Wang, B. Chen and G. Qian, *Nat. Commun.*, 2013, **4**, 2719; (*f*) Z. Chen, Y. Sun, L. Zhang, D. Sun, F. Liu, Q. Meng, R. Wang and D. Sun, *Chem. Commun.*, 2013, **49**, 11557–11559.

4 (*a*) M. D. Allendorf, C. A. Bauer, R. K. Bhakta and R. J. Houk, *Chem. Soc. Rev.*, 2009, **38**, 1330–1352; (*b*) Y. Jiao, J. Wang, P. Wu, L. Zhao, C. He, J. Zhang and C. Duan, *Chem.–Eur. J.*, 2014, **20**, 2224–2231; (*c*) H. Li, W. Shi, K. Zhao, Z. Niu, H. Li and P. Cheng, *Chem.–Eur. J.*, 2013, **19**, 3358–3365; (*d*) P. Wang, J. P. Ma, Y. B. Dong and R. Q. Huang, *J. Am. Chem. Soc.*, 2007, **129**, 10620–10621; (*e*) G. He, D. Guo, C. He, X. Zhang, X. Zhao and C. Duan, *Angew. Chem., Int. Ed.*, 2009, **48**, 6132–6135.

5 (*a*) Y. Cui, B. Chen and G. Qian, *Coord. Chem. Rev.*, 2014, **273–274**, 76–86; (*b*) L. E. Kreno, K. Leong, O. K. Farha, M. Allendorf, R. P. V. Duyne and J. T. Hupp, *Chem. Rev.*, 2012, **112**, 1105–1125; (*c*) Y. Li, S. Zhang and D. Song, *Angew. Chem., Int. Ed.*, 2013, **52**, 710–713; (*d*) Q. Tang, S. Liu, Y. Liu, J. Miao, S. Li, L. Zhang, Z. Shi and Z. Zheng, *Inorg. Chem.*, 2013, **52**, 2799–2801.

6 (*a*) Z. Hu, B. J. Deibert and J. Li, *Chem. Soc. Rev.*, 2014, **43**, 5815–5840; (*b*) Y. Wang, J. Yang, Y. Y. Liu and J. F. Ma, *Chem.–Eur. J.*, 2013, **19**, 14591–14599; (*c*) K. A. White, D. A. Chengelis, K. A. Gogick, J. Stehman, N. L. Rosi and S. Petoud, *J. Am. Chem. Soc.*, 2009, **131**, 18069–18071.

7 (*a*) J. Park, D. Feng and H. C. Zhou, *J. Am. Chem. Soc.*, 2015, **137**, 1663–1672; (*b*) Y. Q. Lan, H. L. Jiang, S. L. Li and Q. Xu, *Adv. Mater.*, 2011, **23**, 5015–5020; (*c*) F. Luo and S. R. Batten, *Dalton Trans.*, 2010, 4485–4488.

8 (*a*) J. An, C. M. Shade, D. A. Chengelis-Czegan, S. Petoud and N. L. Rosi, *J. Am. Chem. Soc.*, 2011, **133**, 1220–1223; (*b*) J. S. Qin, S. R. Zhang, D. Y. Du, P. Shen, S. J. Bao, Y. Q. Lan and Z. M. Su, *Chem.–Eur. J.*, 2014, **20**, 5625–5630.

9 (*a*) Y. P. He, Y. X. Tan and J. Zhang, *J. Mater. Chem. C*, 2014, **2**, 4436–4441; (*b*) M. L. Ma, C. Ji and S. Q. Zang, *Dalton Trans.*, 2013, 10579–10586; (*c*) M. L. Ma, J.-H. Qin, C. Ji, H. Xu, R. Wang, B. J. Li, S. Q. Zang, H. W. Hou and S. R. Batten, *J. Mater. Chem. C*, 2014, **2**, 1085–1093.

10 (*a*) H. Fei, D. L. Rogow and S. R. J. Oliver, *J. Am. Chem. Soc.*, 2010, **132**, 7202–7209; (*b*) Y.-C. He, J. Yang, W.-Q. Kan, H.-M. Zhang, Y.-Y. Liu and J.-F. Ma, *J. Mater. Chem. A*, 2014, **3**, 1675–1681; (*c*) S. R. J. Oliver, *Chem. Soc. Rev.*, 2009, **38**, 1868–1881; (*d*) S. Yang, X. Lin, A. J. Blake, K. M. Thomas, P. Hubberstey, N. R. Champness and M. Schroder, *Chem. Commun.*, 2008, 6108–6110.

11 (*a*) R. Custelcean and B. A. Moyer, *Eur. J. Inorg. Chem.*, 2007, 1321–1340; (*b*) S. Yang, X. Lin, A. J. Blake, G. S. Walker, P. Hubberstey, N. R. Champness and M. Schröder, *Nat. Chem.*, 2009, **1**, 487–493.

12 (*a*) X. Zhao, X. Bu, T. Wu, S. T. Zheng, L. Wang and P. Feng, *Nat. Commun.*, 2013, **4**, 2344; (*b*) Z. Zhu, Y. L. Bai, L. Zhang, D. Sun, J. Fang and S. Zhu, *Chem. Commun.*, 2014, **50**, 14674–14677.

13 (*a*) S. Yang, G. S. Martin, J. J. Titman, A. J. Blake, D. R. Allan, N. R. Champness and M. Schroder, *Inorg. Chem.*, 2011, **50**, 9374–9384; (*b*) S. Yang, S. K. Callear, A. J. Ramirez-Cuesta,

W. I. F. David, J. Sun, A. J. Blake, N. R. Champnessa and M. Schröder, *Faraday Discuss.*, 2011, **151**, 19–36; (*c*) Y. Liu, J. F. Eubank, A. J. Cairns, J. Eckert, V. C. Kravtsov, R. Luebke and M. Eddaoudi, *Angew. Chem., Int. Ed.*, 2007, **46**, 3278–3283; (*d*) S. Huh, T.-H. Kwon, N. Park, S.-J. Kim and Y. Kim, *Chem. Commun.*, 2009, 4953–4955; (*e*) S. Chen, J. Zhang, T. Wu, P. Feng and X. Bu, *J. Am. Chem. Soc.*, 2009, **131**, 16027–16029; (*f*) S. Yang, X. Lin, A. J. Blake, G. S. Walker, P. Hubberstey, N. R. Champness and M. Schröder, *Nat. Chem.*, 2009, **1**, 487–493.

14 G. M. Sheldrick, *SHELXL-97, Programs for X-ray Crystal Structure Solution*, University of Göttingen, Göttingen, Germany, 1997.

15 (*a*) K. Koh, A. G. Wong-Foy and A. J. Matzger, *Angew. Chem., Int. Ed.*, 2008, **47**, 677–680; (*b*) S. Hu, K. H. He, M. H. Zeng, H. H. Zou and Y. M. Jiang, *Inorg. Chem.*, 2008, **47**, 5218–5224.

16 (*a*) A. L. Spek, *J. Appl. Crystallogr.*, 2003, **36**, 7–13; (*b*) P. v. d. Sluis and A. L. Spek, *Acta Crystallogr., Sect. A: Found. Crystallogr.*, 1990, **46**, 194–201.

17 (*a*) M. Du, Z. H. Zhang, L. F. Tang, X. G. Wang, X. J. Zhao and S. R. Batten, *Chem.–Eur. J.*, 2007, **13**, 2578–2586; (*b*) V. A. Blatov, L. Carlucci, G. Ciani and D. M. Proserpio, *CrystEngComm*, 2004, **6**, 377–395.

18 (*a*) S. Z. Li, J. W. Zhao, P. T. Ma, J. Du, J. Y. Niu and J. P. Wang, *Inorg. Chem.*, 2009, **48**, 9819–9830; (*b*) L. P. Sun, S. Y. Niu, J. Jin and L. Zhang, *Eur. J. Inorg. Chem.*, 2007, 3845–3852.

19 (*a*) X. Wei, T. F. Xie, Y. Zhang, D. J. Wang and J. S. Chen, *Mater. Chem. Phys.*, 2010, **122**, 259–261; (*b*) L. Jing, X. Sun, J. Shang, W. Cai, Z. Xu, Y. Du and H. Fu, *Sol. Energy Mater. Sol. Cells*, 2003, **79**, 133–151.

20 (*a*) C. Y. Sun, X. L. Wang, C. Qin, J. L. Jin, Z. M. Su, P. Huang and K. Z. Shao, *Chem.–Eur. J.*, 2013, **19**, 3639–3645; (*b*) Z. Zhu, Y. L. Bai, L. Zhang, D. Sun, J. Fang and S. Zhu, *Chem. Commun.*, 2014, **50**, 14674–14677; (*c*) W. Zhang, J. Zhang, Z. Chen and T. Wang, *Catal. Commun.*, 2009, **10**, 1781–1785; (*d*) R. Zhang, S. Ji, N. Wang, L. Wang, G. Zhang and J. R. Li, *Angew. Chem., Int. Ed.*, 2014, **53**, 9775–9779.